2018

Development of an Adjustable Spiral-shaped Evaporator

Matthias Feiner
Karlsruhe UAS, Institute of Materials and Processes (IMP), matthias.feiner@hs-karlsruhe.de

Michael Arnemann
Karlsruhe UAS, Institute of refrigeration, air conditioning and environmental technology (IKKU), Germany, michael.arnemann@hs-karlsruhe.de

Martin Kipfmueller
Karlsruhe UAS, Institute of Materials and Processes (IMP), martin.kipfmueller@hs-karlsruhe.de

The Development of an Adjustable Spiral-shaped Evaporator

Matthias FEINER[1]*, Michael ARNEMANN[2], Martin KIPFMÜLLER[1]

[1]Karlsruhe UAS, Institute of Materials and Processes (IMP),
76133 Karlsruhe, Germany
matthias.feiner@hs-karlsruhe.de, phone: +49(721) 925-2076
martin.kipfmüller@hs-karlsruhe.de, phone: +49(721) 925-1905

[2]Karlsruhe UAS, Institute of Refrigeration, Air Conditioning and Environmental Engineering (IKKU)
76133 Karlsruhe, Germany
michael.arnemann@hs-karlsruhe.de, phone: +49(721) 925-1842

* Corresponding Author

ABSTRACT

The cooling of high heat flux is becoming increasingly important in technical applications. This is on the one hand due to the fact that the available installation space is becoming smaller and smaller due to progressive miniaturization, on the other hand to the ever-increasing performance, which has to be taken away in technically demanding processes such as Inconel machining. In order to meet this challenge, a new type of evaporator, the swirl evaporator, was developed.
The swirl evaporator is a screw-shaped cylindrical evaporator with an internal diameter between 1 – 3 mm, which is inserted as a blind hole in components with high heat generation. The refrigerant is fed into the blind hole via a concentrically oriented capillary, deflected by 180° in the drilling base and flows out of the evaporator again in a helical way (twist flow) against the inflow direction. The evaporator's design allows a compact size to be achieved, making it suitable for a wide range of technical applications.
To enable a design for industrial needs, a 1-D simulation of the process had been conducted. The simulations showed ideal results for a hydraulic diameter of 2.05 mm and an evaporator length of 15 – 20 mm. According to the simulations an improvement of the energy efficiency of up to 19 % is possible when the mass flow is kept constant for R32. Based on the results of these simulations a design of the test-rig had been developed which allows different screw inserts to be tested with a variable length.
Former experimental studies with R404A show that the average critical heat flux density of spot evaporators with a twist geometry increases by up to 33 % compared with spot evaporators without twist generation. The spot evaporators with swirl flow generation have a distinct, stable overheating zone with high heat flux (Humpfer, 2013).

1. INTRODUCTION

In many mechanical driven technical applications heat must be dissipated as low-value energy. Low-performance processes usually produce little heat, whereas high-performance processes require cooling systems with high cooling performance respectively high heat flux. In many cases, the cooling system represents a bottleneck in the process improvement that must be optimized. This is due to the fact that with high heat flux and the resulting critical wall overheating, the critical heat flux density is exceeded and the cooling process collapses. With spray cooling it is possible to cool with heat flux densities higher than the critical heat flux density attainable with film boiling (Bogdanic *et al*., 2009). For the cooling of e. g. small cylindrical injection moulds, water cooling is no longer sufficient (Steinko and Bader, 2008) and so in Knipping developed and investigated a powerful evaporator called a spot evaporator as part of a dissertation (Knipping, 2018).

The spot evaporator is an evaporator in which the refrigerant flows through the capillary into the evaporator, is deflected at the end face of the blind hole by 180° against the inflow direction and flows partly or completely

evaporated out of the spot evaporator again. It combines spray cooling and evaporation of the refrigerant in the pipe flow. Spot evaporators have a length of 10 – 50 mm, an inside diameter of 1 – 3 mm and a capillary diameter of 0.8 mm outside and 0.5 mm inside (Knipping, 2018). The schematic sketch of the spot evaporator with the corresponding heat flow $\dot{Q}$ and mass flow $\dot{m}$ is shown in Figure 1.

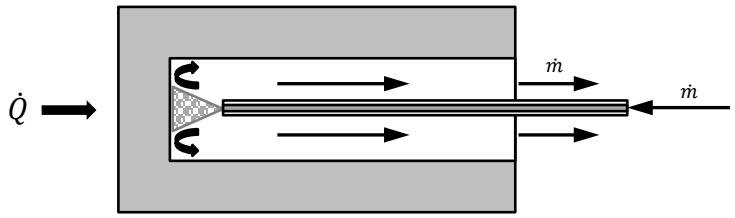

Figure 1: Spot evaporator

Potential fields of application can be seen in the cooling of linear motors or, as already mentioned, in tools for plastic injection molding (Knipping *et al*., 2015) as well as in the milling of materials such as Inconel 718, (Knipping *et al*., 2014). The advantages of this system are not only its simple manufacturability, but above all its high heat flux densities and precise heat dissipation. The disadvantages are the poor controllability and still shows energetic optimization potentials, since in the operating state usually not all refrigerant evaporates, so a post-evaporator is also necessary.

2. STATE OF THE ART

The spot evaporator holds potential for improvement by inserting a swirl-shaped return of the refrigerant. In this context Humpfer investigated two different swirl generating evaporator geometries for their improvement potentials with regard to cooling capacity. A type of spring insert was compared with a screw insert as shown in Figure 2. He named the design “swirl evaporator”. The swirl evaporator represents a further development of the spot evaporator. It combines the spray cooling of the spot evaporator with a downstream swirl component and proves to be promising with regard to an increase in output. The swirling geometry causes centrifugal acceleration, which causes the refrigerant to rotate around the longitudinal axis. In order to cool with high heat flux, there must be enough vaporizable material on the evaporator surface, which is why the critical heat flux is increased by the swirl component. Humpfer's experiments show that, in addition to the twisting movement, the mass flow has the greatest effect on an increased critical heat flux. However, if a spot evaporator with the same mass flow is compared to the swirl flow, the maximum evaporator capacity can be increased by up to 33 % for R404A (Humpfer, 2013). The heat transfer in film boiling has been greatly increased when using a screw insert. Humpfer assumes that the cooling capacity can be further improved; no quantification of this statement has yet to be carried out.

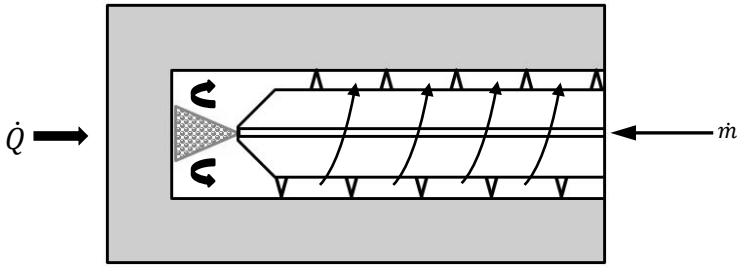

Figure 2: Schematic sketch of a swirl evaporator, screw inserted

Based on the first experiments of Humpfer, the influence of the spiral geometry should be investigated. In order to enable dynamic cooling with adjustable overheating adapted to the power requirement (like a thermal expansion valve), the screw engagement length is variable. In a later project stage, the screw engagement length is to be set automatically.

As the total quantity of fluorinated greenhouse gases available in the European Union should be drastically reduced by 2030 by Regulation No. 517/2014 and as the total quantity was already reduced to 63 % of the annual average

consumption between 2009 and 2012 on 1 January 2018, R404A can no longer be used (EU Regulation 517, 2014**)**. Due to the lower GWP of R32 this refrigerant can be an alternative, even if the safety class is A2L (ISO-817, 2014).

For a better overview of the two circular processes, these are shown schematically in Figure 3. In both processes, the superheated refrigerant is raised to the upper pressure level by the piston compressor (1). In the condenser heat gets rejected from the refrigerant and it condenses (2). After this the liquid refrigerant expands isenthapically in the capillary (3), which causes the temperature of the refrigerant to drop. The active area of both evaporators can be divided into a spray cooling area (4) and a ring flow area (5a) for the spot evaporator or helical pipe flow area (5b) for the swirl evaporator. In principle, the pressure loss in the helical pipe flow area of the swirl evaporator is bigger than in the ring flow area of the spot evaporator. When leaving the ring flow area of the spot evaporator, the refrigerant is located in the two-phase region and is superheated via the post evaporator (6). After superheating, the pressure level is raised by the compressor and the circuit starts again.

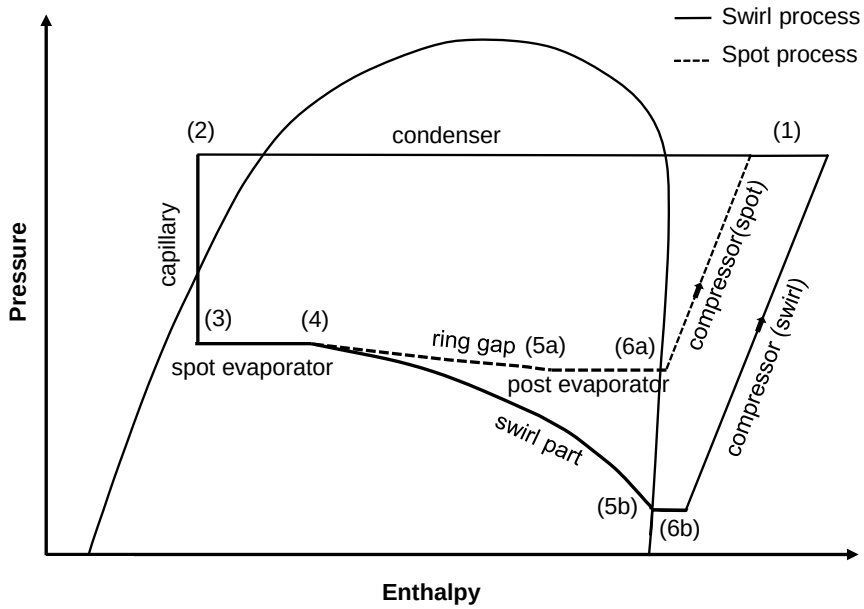

Figure 3: Cycle process diagram

3. DESIGN OF A SWIRL EVAPORATOR

To determine the influence of different swirl geometries on the process, a test trial was developed. In addition to the relevant basics, the previous studies on the spot and swirl evaporator are also described and the design of the swirl evaporator is carried out. The core piece is a simulation of the pressure loss on the basis of which the geometric quantities of the evaporator were estimated. Subsequently, a functional and production-ready design was developed. To get a rough idea in which dimensions the test carrier has to be designed, the pressure loss in the helical return path has to be determined. The optimum between running length (i.e. the helical return path of the refrigerant) and hydraulic diameter must be found.

First of all, the mass flow $\dot{m}$, the inlet temperature T_{in} and the inlet pressure p_{in} of the refrigerant are important input variables. During operation of the given system, the pressure, thus the density, and thus the mass flow of the refrigerant, will be adjusted to the settings in the system. However, since the system characteristics have not yet been investigated, constant input values are assumed for simplicity. The lumped capacitance method is also used for the design.

A simulation was carried out to obtain indications as to how the test stand of the swirl evaporator should be designed. It is important to know the maximum screw engagement length and the hydraulic diameter of the screw threads through which the refrigerant flows. For the estimate of the thermal states, the approach of a 1-D simulation was chosen. Segments were created along this dimension to represent the course of the thermal quantities along the path. The relationships of the pressure loss are based on empirical relationships and the heat input on theoretical

relationships. It is considered mass conservation and the system is considered stationary. From the outside, the system receives a heat input $\dot{Q}$, which depends on the heat transfer coefficient α and on the wall overheating $\Delta\vartheta$. This heat is absorbed by the refrigerant and is reflected in an increase in the steam quality x. The increase in steam quality results in an increase in speed. At the same time there is a pressure loss that depends on the steam quality, the volume flow and the pressure. It turns out that a correlation for the pressure loss can be used as the core of the simulation calculation. For the calculation of the pressure loss in the helical pipe section, considerations were first made for a possible analytical solution. However, these considerations were not pursued further due to the very great effort involved and the fact that no analytical approaches to two-phase helical pressure loss for R32 have yet been published. For the first estimates of the pressure loss in the helical pipe section, Humpfer (Humpfer, 2013) has taken a correlation for the two-phase pressure loss in a straight pipe from the software EES. Fsadni and Whitty conducted a research on pressure losses in multiphase systems and found that a curved pipe has a much greater pressure loss than a straight pipe Fsadni and Whitty, 2016). Therefore, it was decided to use a correlation for a curved pipe.

When flowing through an elbow, the centrifugal force acts on the fluid as with a helical pipe. With the associated adhesive forces, two vortices are formed, which have a significant influence on the flow pressure loss. At the same time, the pressure loss depends on the position and direction of the manifold outlet. Therefore, the idea of estimating the pressure loss through a series of manifolds proves to be unhelpful, since the inlet and outlet geometry of a manifold strongly influences the formation of the empirical equations.

Guo *et. al* has shown the relationship between pressure losses as a function of steam quality, mass flow density, pressure and viscosity. The geometries and the pressure for which he did these experimental investigations are most suitable for the present case. However, water was used as fluid, which could later lead to larger deviations (Guo *et al.*, 2001). The model can be parameterized for the refrigerant in question when carrying out experiments as part of the further progress of this project. In the correlation of Guo *et al.*, the multiphase pressure drop can be represented by a correlation with the single-phase pressure drop:

$$\Delta p_{\mathrm{tp}} = \Phi_l^2 \, \Delta p_l \tag{1}$$

Δp_l is the single-phase pressure drop and Φ_l^2 is the correlation for the two-phase pressure drop. The two-phase correlation results from the following semi-empirical context:

$$\Phi_l^2 = \psi_1 \cdot \psi \cdot \left[1 + x\left(\frac{\rho_l}{\rho_{\mathrm{g}}} - 1\right)\right] \tag{2}$$

The mass flow density G is used to differentiate between two flow regimes that with different equations give different correlations for ψ. For $G \leq 1000$ the relationship is

$$\psi = 1 + \frac{x(1-x)\left(\frac{1000}{G} - 1\right)\frac{\rho_l}{\rho_{\mathrm{g}}}}{1 + x\left(\frac{\rho_l}{\rho_{\mathrm{g}}} - 1\right)}. \tag{3}$$

For $G > 1000$ the equation is

$$\psi = 1 + \frac{x(1-x)\left(\frac{1000}{G} - 1\right)\frac{\rho_l}{\rho_{\mathrm{g}}}}{1 + (1-x)\left(\frac{\rho_l}{\rho_{\mathrm{g}}} - 1\right)}. \tag{4}$$

The coefficient ψ_1 contains the critical pressure and the geometrically important relationships of the hydraulic diameter and the radius of curvature.

$$\psi_1 = 142.2\left(\frac{p}{p_{\mathrm{crit}}}\right)^{0.62}\left(\frac{D}{R}\right)^{1{,}04} \tag{5}$$

In this way, the selected correlation for the pressure drop is built up. Figure 4 shows a section of the geometry that has been optimized. The bore diameter is $D = 5$ mm. This size was determined so that the other sizes can be related to it. Diameter d represents the hydraulic diameter of the spiral flow channel. The radius R results from the distance of the center of the flow channel from the longitudinal axis and the length of the evaporator L results from the series of individual segments. The small distance between the individual flow channels is neglected.

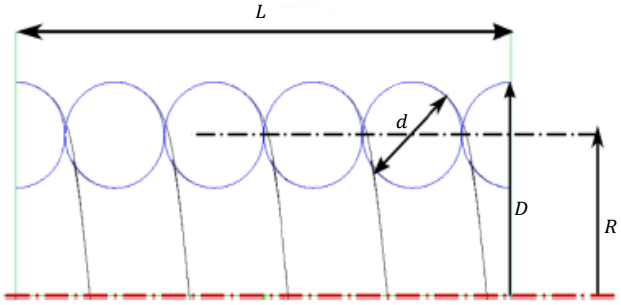

Figure 4: Geometric sizes of the swirl insert

Within one segment it was assumed that it is an adiabatic volume entity. At this point, the pressure loss is calculated using the correlations described above. The previous pressure minus the pressure loss results in the new pressure. The heat flow into a segment is then calculated using the length of the volume piece, the hydraulic diameter and the heat transfer coefficient. Between the segment boundaries, the absorbed heat results in an increased enthalpy difference, which is reflected in an increase in steam quality. Due to the changed steam quality, a new pressure arises again. Figure 5 shows how the simulation model of the pressure loss in the helical return path of the refrigerant is set up.

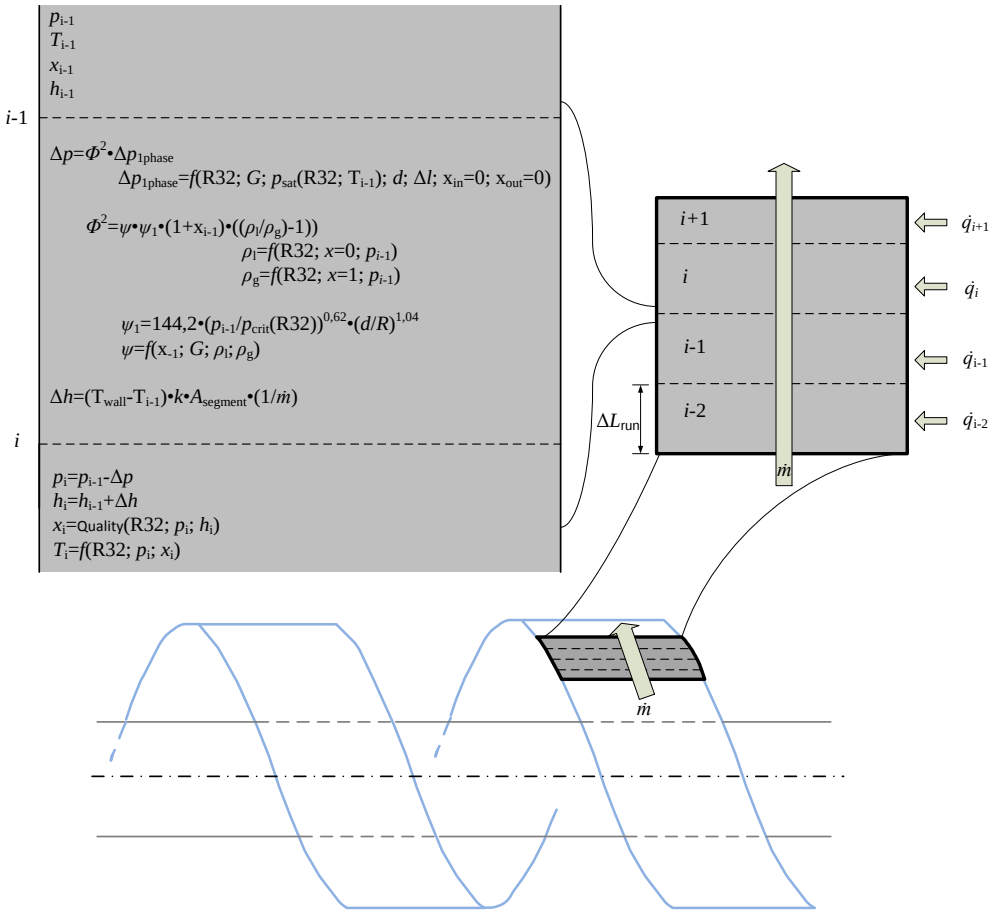

Figure 5: Simulation model of the pressure loss in the helical return path of the refrigerant

The pressure drop within the Swirl Evaporator should not exceed 0,4 MPa (Humpfer, 2013). For this reason, the maximum pressure drop was selected as the abort criterion for the simulation. It turns out that with a steam quality of $x = 1$ the length should not be increased further, as all refrigerant has evaporated. For reasons of numerical stability, the simulation program achieves the so-called maximum steam quality from a steam quality of $x = 0.99$.
There is a conflict of objectives when designing the evaporator. On the one hand, the hydraulic diameter of the threads should not be too small, so that the pressure loss is minimized. On the other hand, an increase in the hydraulic diameter means fewer threads, which means that not all refrigerant evaporates. Therefore, a compromise was sought in the simulation for a hydraulic diameter in which all refrigerant evaporates without the pressure loss exceeding the maximum permissible value.
Two termination criteria must be selected for the simulation of the maximum run length. Figure 5 shows the maximum running length over the hydraulic diameter for both demolition criteria. The first criterion is the maximum pressure loss $\Delta p_{\max}$ of 0.4 MPa and the second criterion is the steam quality x, which should reach 0.99. Ideally, both criteria are achieved simultaneously. The value $L = 100$ mm is the upper limit value in the simulation. At the intersection of the two curves with a hydraulic diameter of $d = 2.05$ mm and a run length of $L_{\text{run}} = 52.85$ mm, which corresponds to a swirl length of $L = 14.09$ mm (cylinder length, bore depth). The result of the simulation can be seen in Figure 6 at the intersection of both curves. Since simplified assumptions were made in the simulation, a bore depth of 40 mm is chosen in the test bench which can be continuously adjusted from 1 to 40 mm to test various parameters.

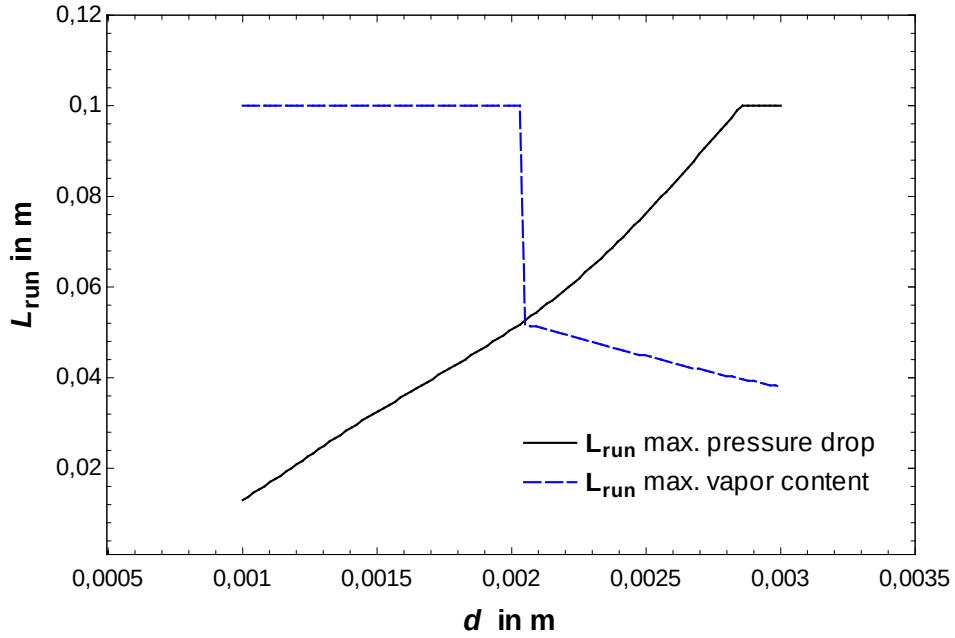

Figure 6: Result of the simulation

The test stand for the measurements of the swirl evaporator is located on the refrigerant test stand at the Institute of Material and Processes (IMP) at the University for Applied Sciences Karlsruhe, Germany. In the current configuration, the test stand is operated with the refrigerant R32 without any oil in the cycle. An overview is given in Figure 7. A detailed description is given in (Knipping, 2018). A photograph of the test stand is shown in Figure 8.

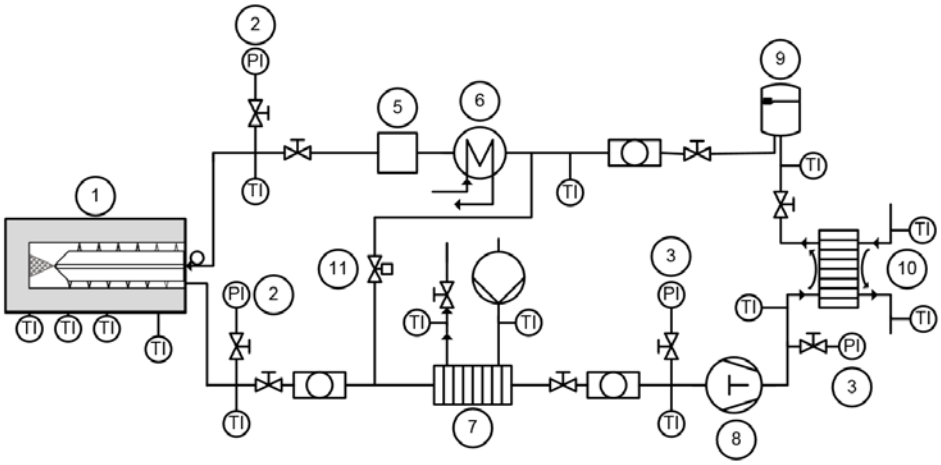

Figure 7: Experimental setup for heat transfer investigation at high heat fluxes (modified from Knipping, 2018)

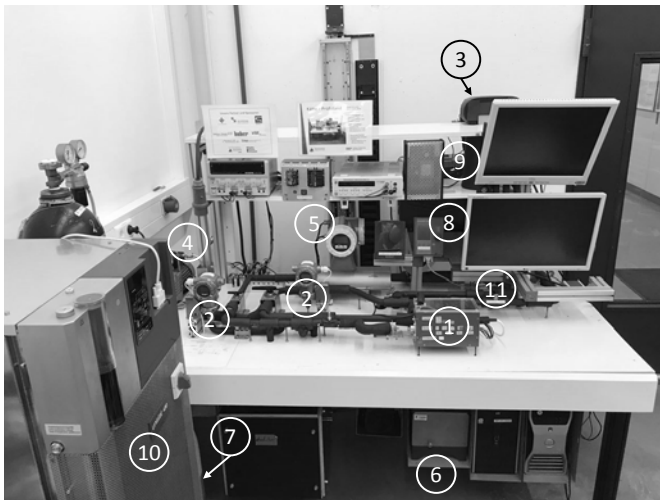

Figure 8: Photograph of the test stand

In Table 1 the parts of the experimental setup are described. Heat is supplied from the outside to the heat sink via heating sleeve. On the wall surface, where the refrigerant impinges, a phase transition of the liquid to the gaseous one takes place.

Table 1: Parts of the experimental setup

1	Sample chamber with swirl evaporator	7	Post-evaporator
2	PI pressure sensor (F = 0.05 % o. m. v.)	8	Compressor (oil-free)
3	PI pressure sensor (F = 0.1 % o. m. v.)	9	Refrigerant assembler
4	Vacuum pump	10	Thermostat
5	Mass flow meter	11	Step motor controlled expansion valve
6	Thermostat	TI	Thermocouples Type J

4. DESIGN IMPLEMENTATION

Figure 9 shows the design of the swirl evaporator with variable screw engagement length that will be used for the experimental setup. It does not yet provide a controllability of the screw engagement length during the test. It should

be possible to vary the screw engagement length manually using an adapter in order to parametrize the simulation model in several experiments. The adapter is sealed by an O-ring and held in position at the same time.

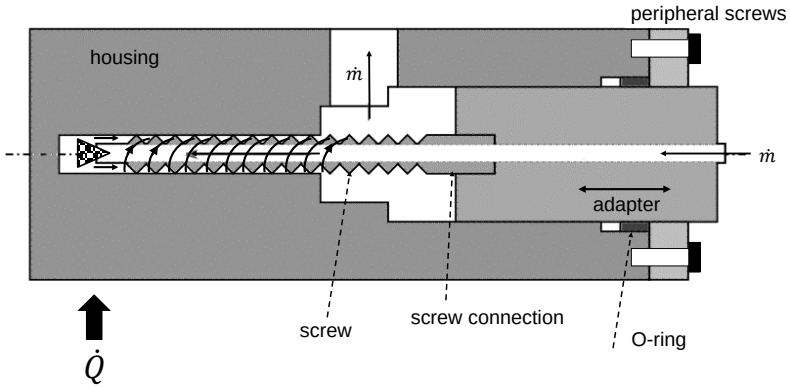

Figure 9: Swirl evaporator with variable screw engagement length

If the peripheral screws are loosened, the adapter can change its position because the O-ring returns to its original state and no longer presses in the adapter. The cavity in front of the adapter contains a different volume depending on its position. If the system is flooded with refrigerant, this cavity will fill and plays no further role in the system dynamics. In addition, this space, in the form of a larger diameter, also serves to keep the outlet conditions almost constant. The adapter itself offers the possibility to maintain the remaining test setup and to carry out tests with different hydraulic diameters and other screw geometries.

A non-oil-lubricated seal in the form of two O-rings is used to ensure the sealing of the refrigerant to prevent the penetration of lubricating films into the refrigeration circuit. The measuring device is also free-standing in order to reduce the influence of external disturbances and to concentrate the heat conduction path on the refrigerant inside. Each additional bearing position deteriorates the thermal insulation. The bearing location on the U-profile is therefore as far away from the heat input of the heating sleeve as possible.
Five temperature-measuring points are provided for measuring the temperature curve from spray cooling to the exit from the swirl. Another important parameter for validating the simulation model is the pressure drop from the screw inlet to the screw outlet. Therefore, two pressure-measuring points were provided in the heat sink. To minimize further external influences, the construction is located in an insulated housing, as shown in Figure 10.

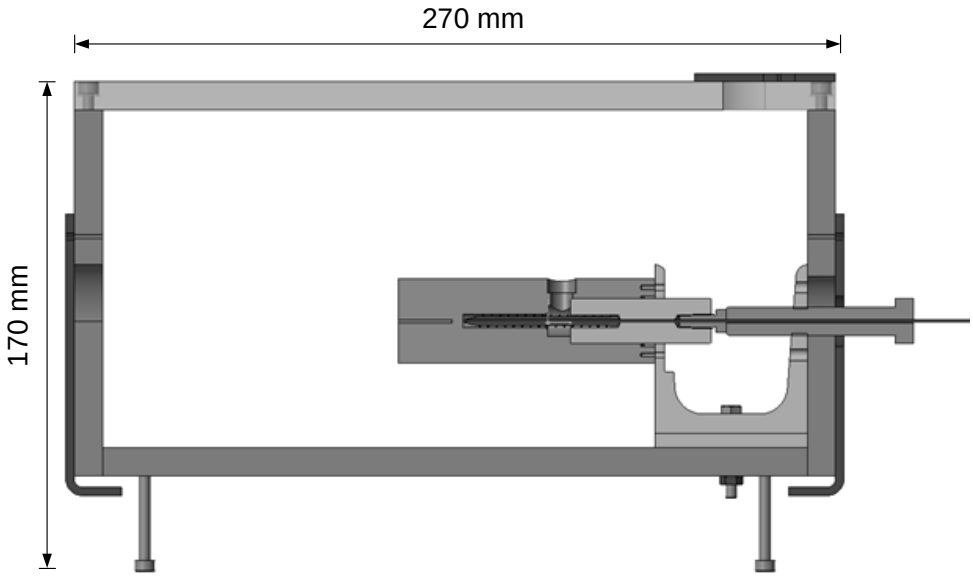

Figure 10: Sample chamber with swirl evaporator

5. CONCLUSIONS

In the context of this work, research was carried out into possibilities of describing the pressure loss within the swirl evaporator:

- A simulation approach was chosen in which the maximum running length and the corresponding steam quality can be determined for different diameters.
- The maximum running length and thus also the evaporator length increase over the diameter.
- With a diameter of approx. 2.05 mm, the maximum steam quality and maximum pressure loss are achieved simultaneously.
- The optimum is in this range if the mass flow is fixed.
- Due to the higher steam quality, which results in a larger enthalpy difference, a performance increase of approx. 19 % compared to the spot evaporator is expected at a constant mass flow.
- Since the mass flow is lower due to the greater pressure losses, the actual increase is less than 19 %.
- The exact change in the mass flow due to the swirl evaporator in the refrigeration circuit could not be determined in the course of this work. Thus, an experimental setup to investigate the problem has been set up. It provides an adapter for different screw geometries and allows a variable track length for the refrigerant.
- This allows different screw geometries to be compared and the optimum length for the respective geometry to be determined.
- A stop enables reproducibility of the measurements.
- By using two seals, similar to a stuffing box, it is possible to seal the circuit both gas-tight and oil-free.
- Environmental influences are reduced by the freestanding geometry of the heat sink with the heating sleeve and the reconstructed plastic housing.
- Relevant state variables can be measured by pressure and temperature measuring points.

NOMENCLATURE

d	diameter	(m)
L	length of the evaporator	(m)
p	pressure	(Pa)
p_{crit}	critical pressure	(Pa)
R	radius	(m)
ψ	correlation factor	(–)
tp	two-phase	(–)
L_{run}	running length	(m)
x	steam quality	(–)

REFERENCES

Bogdanic, L., Auracher, H. u. Ziegler, F. (2009): *Two-phase structure above hot surfaces in jet impingement boiling. In: Heat and Mass Transfer, 45*, p. 1019–1028

Fsadni, A. M.; Whitty, J. P.: *A review on the two-phase pressure drop characteristics in helically coiled tubes*. Applied Thermal Engineering 103 (2016), S. 616–638

Guo, L., Feng, Z. u. Chen, X.: *An experimental investigation of the frictional pressure drop of steam–water two-phase flow in helical coils*. International Journal of Heat and Mass Transfer 44 (2001) 14, S. 2601–2610

Humpfer, F. (2013): *Erhöhen des Kühlvermögens von Spot-Verdampfern bei hohen Wärmestromdichten durch Erzeugung einer Drallströmung* (Unpublished master's thesis). Hochschule Karlsruhe – Technik und Wirtschaft, Karlsruhe, Germany

ISO 817: 2014-05 Refrigerants - Designation and safety classification

Knipping, T. (2018): *Kühlen kleiner Kavitäten mit verdampfenden Fluiden* . DKV-Forschungsbericht, No. 88

Knipping, T., Arnemann, M., Hesse, U., Humpfer, F. u. Ganz, M. (2012): Forced bulk boiling at high heat fluxes. *Proceedings of the International refrigeration and air conditioning conference, Purdue*, paper No. 2586

Knipping, T., Arnemann, M., Hesse, U. u. Humpfer, F. (2014): Experimental analysis of twisted shaped spot evaporators at high heat fluxes. *Proceedings of the International refrigeration and air conditioning conference, Purdue*, paper No. 2587

Knipping, T., Humpfer, F., Arnemann, M. u. Hesse, U. (2015): *Untersuchungen zu Drall-Spot-Verdampfern bei hohen Wärmestromdichten. Kälte Luft Klimatechnik. Januar-Februar* (1-2), p. 28-31

Regulation (EU) No 517/2014 of the European Parliament and of the Council of 16 April 2014 on fluorinated greenhouse gases and repealing Regulation (EC) No 842/2006

Steinko, W. u. Bader, C. (2008): *Optimierung von Spritzgießprozessen*. München: Hanser